Progress In Electromagnetics Research M, Vol. 73, 91–100, 2018

Design of New Broad Stop Band (BSB) Lowpass Filter Using Compensated Capacitor and Π-H-Π DGS Resonator for Radar Applications

Ahmed Boutejdar[1, *], Mouloud Challal[2], and Soumia El Hani[3]

Abstract—In this paper we present a new compact microstrip lowpass filter using a Π-H-Π-DGS resonator etched in the ground plane and two patches compensated capacitors placed on the top layer. Two DGS shapes are electromagnetically coupled. The proposed lowpass filter has shown improvement by adding a square microstrip to the single DGS resonator. The design procedure is validated using the commercial full-wave EM MoM simulator Microwave Office. Simulated as well as measured results exhibit sharp roll-off (ξ) of 34 dB/GHz and create a transmission zero at around 4 GHz with attenuation level −34 dB near the passband. On the other hand, the proposed LPF has shown wide stopband bandwidth with rejection better than −20 dB from 3.5 GHz up to 11.5 GHz, while the size of the whole structure is smaller (20 mm × 20 mm). Finally, the proposed filter structure was fabricated and measured. The measurements are in a good agreement with the simulated results.

1. INTRODUCTION

In recent years, the demand for compact microstrip lowpass filters has increased due to the recently expanding microwave and mobile communication systems. So far, a few effective techniques [1–9] have been successfully developed to miniaturize the filter size and suppress the spurious harmonic passband without increasing the number of periodic structures. The lowpass filters are of key importance for the radio frequency engineer, since they are currently used in communication applications to remove undesired harmonics or spurious mixing products and allow signals with certain frequencies to pass. Additionally, the performance of compact design, low insertion loss in the passband and sharpness in transition domain are necessary to meet the requirements. Much effort has been made to develop a variety of compact microstrip lowpass filters. In order to improve the sharpness and effectiveness of spectrum utilization, filters with several attenuation poles are required. A Hi-Lo technique has been proposed to achieve a single transmission zero at high stopband [10]. The disadvantages are complicated fabrication and big loss along the thin microstrip. Another two transmission zeros lowpass filter has been realized using only DMS technique, but the radiation caused from the DMS-corners and which could not be compensated has negatively influenced the results [11]. For these previous purposes, other researchers have used stepped impedance resonators (SIRs) [12–15]. In the practical application, one of the requisite qualities is sharp passband to stopband transition, but the filters mentioned above all have gradual cutoff response. The rejection features can be improved by increasing the number of cascade resonators, which, however, leads to a high passband insertion loss (IL) and larger physical size of the filter.

Received 26 June 2018, Accepted 24 August 2018, Scheduled 13 September 2018
* Corresponding author: Ahmed Boutejdar (boutejdar69@gmail.com).
[1] German Research Foundation (DFG), Braunschweig-Bonn, Germany. [2] University Boumerdes, Institute of Electrical and Electronic Engineering, Boumerdes, Algeria. [3] Mohammed V University in Rabat, ENSET, Rabat, Morocco.

The DGS components are the dominant technology which can provide size reduction and has the capability of suppressing harmonics and spurious signals [16–20]. The DGS, evolved from EBG structures, can be applied to various kinds of components such as lowpass filters and bandpass filters as well as RF phase shifters. DGS can be etched periodically or non-periodically cascaded shapes in the ground of a planar transmission line. DGS causes disturbance in a shield current distribution in the metallic ground plane. This disturbance leads to change of characteristics of a transmission line such as line capacitance and inductance. Thus, DGS elements are equivalent to the LC circuit [21, 22].

To eliminate this disadvantage and thus to manufacture a lowpass filter, which is compact and useful in personal communication systems, we suggest a class of lowpass filters which consist of a combination of defected ground structures (DGS) and compensated patch capacitors. Two microstrip capacitors are placed near each other and are connected with SMA-connectors through a 50 Ω feed line. Two electromagnetically coupled neighbour DGS elements are etched in the ground plane.

In this paper, we introduce a new technique to obtain an ultra-wide reject band LPF using a new Π-H-Π-DGS resonator. The new L-band-lowpass filter is designed, optimised, fabricated, and measured. Use of DGS technique allows us to easily control the coupling effect and suppress higher harmonics.

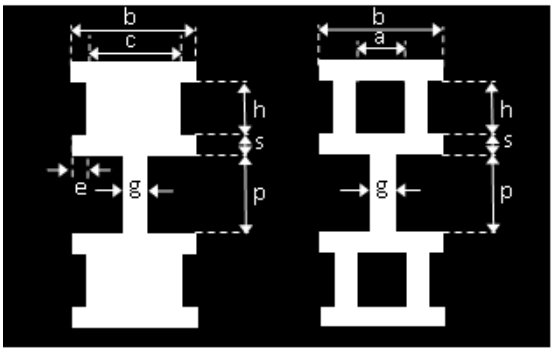

Figure 1. Schematic view of the Π-H-Π-DGS cell. Left: Conventional DGS, right: improved DGS.

In order to tune the desired transmission zeros or attenuation poles which determine the sharpness of the transitions of the stop domain, the main window (DGS head) is optimized. The proposed filter shows a large reject band, good sharpness factor and small insertion loss in the passband. The AWR software was employed in the full wave simulations. Finally, the measured results exhibit good agreement with the simulations.

2. CHARACTERISTICS OF THE Π-H-Π-DGS RESONATOR

The simple Π-H-Π-DGS slot is etched in the ground plane of the microstrip line and consists of two inductive heads, which are connected to each other through a thin slot channel, as shown in Figs. 1 and 2. The etched slot head corresponds to an equivalent inductance, while the channel between the two arrowheads corresponds to an equivalent capacitance. All the dimensions of the proposed Π-H-Π-DGS slot are depicted in Table 1.

Figure 3 a simple equivalent circuit approach, which is based on Tchebycheff's π-network, where C_S is the sum of the capacitances in the ground and L_s the parallel inductance to C_S. The parallel

Table 1. Dimensions of the defected ground structure (DGS)-element.

Dimensions of DGS-unit	a	b	h	S	p	g	c	e
values (mm)	2.0	5.0	1.7	1.2	2.8	1.2	4.0	0.6

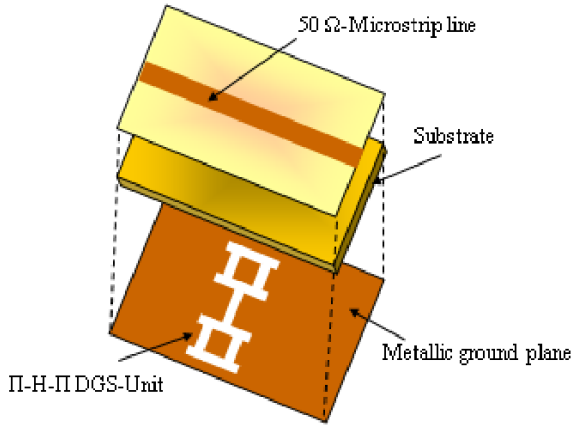

Figure 2. The 3D view of the Π-H-Π-slot in the ground plane.

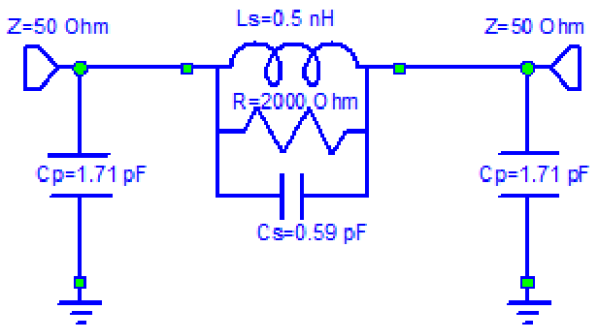

Figure 3. Equivalent circuit model of the proposed Π-H-Π-DGS unit.

capacitance C_P, between the microstrip feed and the metallic ground, describes the influence resulting from the fringing field around the DGS unit.

In order to improve the filter features and to ensure a high degree of freedom to control the results without any additional elements, while maintaining the size as before, the classical DGS is transformed to Π-H-Π-DGS by adding a small rectangular metal from the rectangular slot-head. The substrate properties used in the simulations are: $\varepsilon_r = 3.38$ and the thickness h of 0.813 mm. The Π-H-Π-DGS slot is modelled as a parallel LC resonator as shown in Fig. 3 [10]. The circuit model is devised using a microwave office simulator. The equivalent circuit parameters can be calculated from the S-parameters based on the electromagnetic (EM)-simulation. S_{21} and S_{11} will be used to compute the resonance and cutoff frequencies of the circuit using AWR simulator. The required parameters can be defined by using the relation between the S-$ABCD$-parameters and Y-parameters as follows:

$$A = \frac{(1+S_{11})(1-S_{22})+S_{12}S_{21}}{2S_{21}} = 1+\frac{Y_p}{Y_s} \tag{1}$$

$$B = \frac{(1+S_{11})(1+S_{22})+S_{12}S_{21}}{2S_{21}} = \frac{1}{Y_s} \tag{2}$$

$$C = \frac{1}{Z_0}\frac{(1-S_{11})(1-S_{22})-S_{12}S_{21}}{2S_{21}} = 2Y_p+\frac{Y_p^2}{Y_s} \tag{3}$$

$$D = \frac{(1-S_{11})(1+S_{22})+S_{12}S_{21}}{2S_{21}} = 1+\frac{Y_p}{Y_s} \tag{4}$$

Here, Y_S and Y_P from Fig. 3 show the series and parallel admittances of the π-equivalent circuit, while Z_0 represents the characteristic impedance of the transmission line.

$$Z_s = \frac{1}{Y_s} = B = \frac{RZ_{LC}}{R+Z_{LC}}, \quad R\to\infty \tag{5}$$

$$Z_s = \frac{RZ_{LC}}{R\left(1+\dfrac{Z_{LC}}{R}\right)} = \frac{Z_{LC}}{\left(1+\dfrac{Z_{LC}}{R_{\to\infty}}\right)} = \frac{Z_{LC}}{(1+\to 0)} \tag{6}$$

$$Z_s = Z_{LC} = \frac{j\omega L_s * \dfrac{1}{j\omega C_s}}{j\omega L_s + \dfrac{1}{j\omega C_s}} = \frac{j\omega L_s}{1-\omega^2 L_s C_s} \tag{7}$$

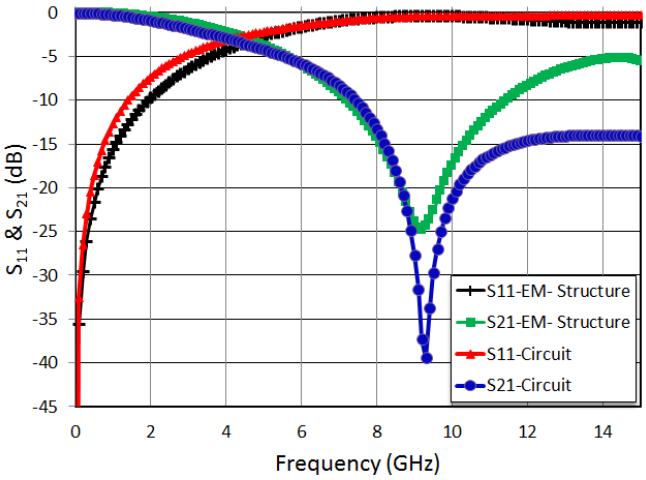

Figure 4. Comparison between the EM- and circuit simulation results of the Π-H-Π element.

$$Y_{LC} = Z_{LC}^{-1} = \frac{1-\omega^2 L_s C_s}{j\omega L_s} = j\left(\omega C_s - \frac{1}{\omega L_s}\right) = jB_{LC} \tag{8}$$

$$B_{LC}\,|_{\omega=\omega_c} = \omega_0 C_s \left(\frac{\omega_c}{\omega_0} - \frac{\omega_0}{\omega_c}\right) \tag{9}$$

$$C_s = \frac{B_{LC}}{\omega_0\left(\dfrac{\omega_c}{\omega_0} - \dfrac{\omega_0}{\omega_c}\right)} \text{ with } \omega_0^2 = \left(\frac{1}{L_s C_s}\right) \tag{10}$$

$$L_s = \left(\frac{1}{\omega_0^2 C_s}\right) \tag{11}$$

$$Y_p = \frac{A-1}{B} = \frac{1}{R_p} + jB_{RC} \approx jB_{RC} = j\omega C_p \tag{12}$$

$$\text{by } \omega = \omega_c \rightarrow C_p = \frac{B_{RC}}{\omega_c} \tag{13}$$

where f_0 is the pole frequency, and f_c is the 3 dB cutoff frequency, which could be extracted from S-parameter response (see Fig. 4) obtained using Microwave Office EM simulators. The EM simulations have been performed for different values of the DGS slot areas and equivalent inductance and capacitance have been calculated using Eqs. (10) and (11). The values of the cutoff frequency f_c and resonance frequency f_0 can be calculated from the transmission characteristics of the Π-H-Π-DGS resonator. The simulation results of the DGS slot show one-pole bandstop characteristics as depicted in Figs. 5, 6 and 7. The dependence of the gap width g of the proposed DGS slot on the cutoff and the resonance frequencies is shown in Fig. 5. If the remaining dimensions are kept constant, while only the parameter g varies from 0.5 mm to 2.15 mm, this leads to increase of the resonance frequency from 7 GHz to 8.9 GHz, and it is easy to control the positions of attenuation pole in a close frequency range, while the cutoff frequency does not undergo a significant change. The same experiment has been carried out by keeping all parameters constant while only the parameter p, length of the gap (channel), varies from 1 mm to 5.5 mm. As before the cutoff results do not undergo interesting changes whereas on the contrary, the resonance frequencies decrease from 9 GHz to 5 GHz. This allows easily controlling the positions of attenuation pole, which shifts to lower frequencies over a large frequency range (see Fig. 6).

The idea behind this study is adjusting the DGS dimensions in order to reach the optimal results. The variation of gap-width-length equivalent to the change of the capacity of the structure leads to a control of the position of the resonance frequency over a large frequency range. As shown in Fig. 7, by changing the area of DGS we would have a desired pole over a wide range of frequencies from 6.5 GHz to 9 GHz. Moreover, by altering other dimensions of DGS unit the attenuation pole frequency will change

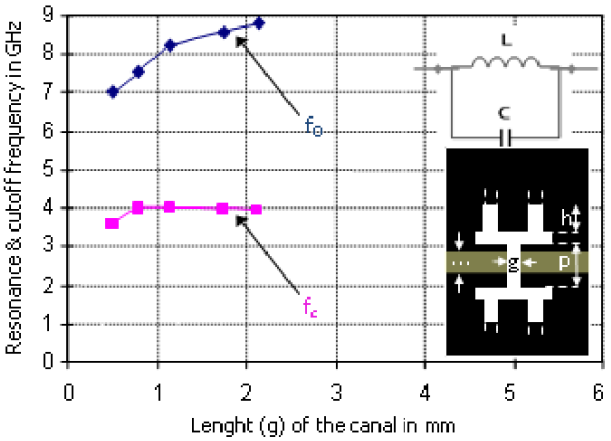

Figure 5. The cut-off and resonance frequencies versus the channel length g of Π-H-Π-DGS resonator.

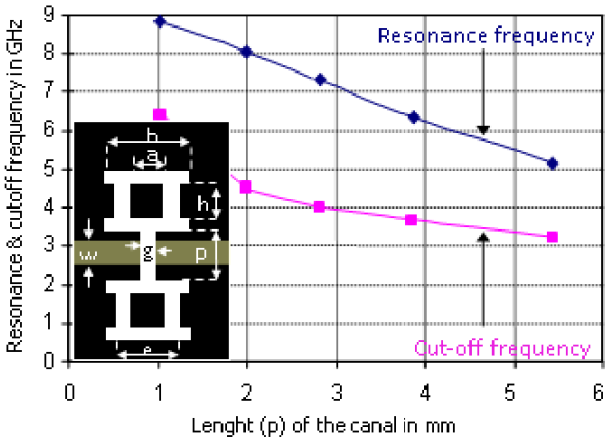

Figure 6. The cut-off (f_0) and resonance (f_c) frequencies versus the channel width p of Π-H-Π-DGS resonator.

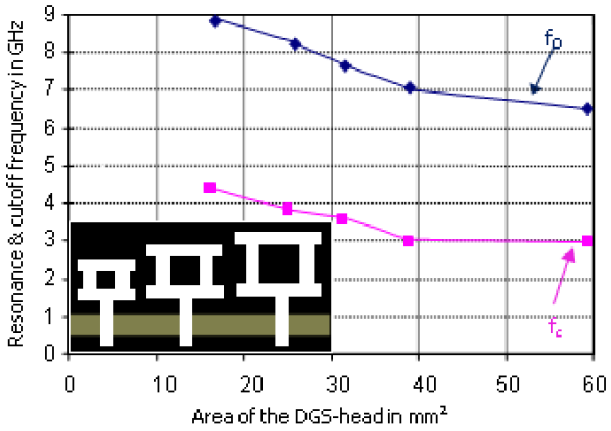

Figure 7. The cut-off (f_0) and resonance (f_c) frequencies versus the head-area of Π-H-Π-DGS resonator.

as well. These features can be used to realise devices with tunable electrical properties. In Fig. 7 we can see that increasing the length area causes a noticeable decrease in the attenuation pole frequency, due to an increase in the inductance property of the slot.

3. DESIGN AND OPTIMIZATION OF THE PROPOSED (BSB) LOW PASS FILTER

In order to show the effectiveness of the proposed Π-H-Π-DGS shape, two three-pole LPFs have been designed, optimized and simulated. The EM coupling between the two DGSs leads to an improvement of the stopband, while the added capacitors on the top layer minimise the loss in the passband (see Fig. 8). The added rectangular metal into the head of the DGS resonator increases the DGS-capacitance and thus improves the compactness of the filter structure (see Fig. 9). The simulation results of this proposed LPF were obtained using Microwave Office as shown in Fig. 10. The substrate used was Rogers RO4003 with dielectric constant of 3.38, thickness of 0.813 mm and dielectric loss tangent (δ) = 0.0027. The dimensions of the LPF and the developed LPF are listed in Table 1. The dimensions of compensated patch capacitor are: length $(d_1 - g_1)/2 = 4.75$ mm where $d_1 = 11$ mm and $g_1 = 1.5$ mm and the width $(d_2) = 3.5$ mm. The coupling distance between the two DGS neigbours is $g_2 = 2$ mm. The simulated results are shown in Fig. 10. As depicted in Fig. 10, the designed LPF structures have cutoff frequencies

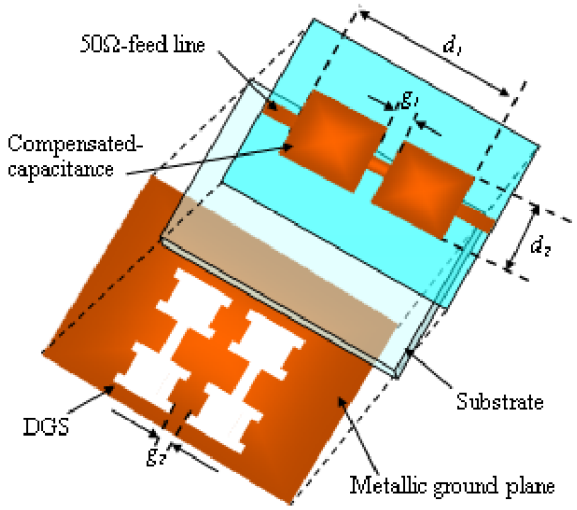

Figure 8. The 3D view of the proposed Π-H-Π LPF.

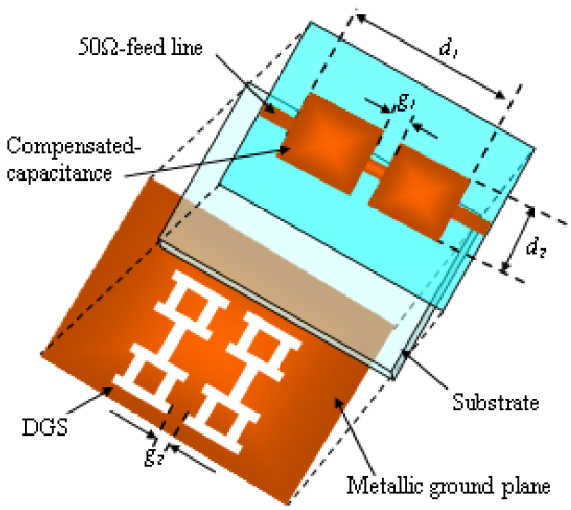

Figure 9. The 3D view of the improved Π-H-Π LPF.

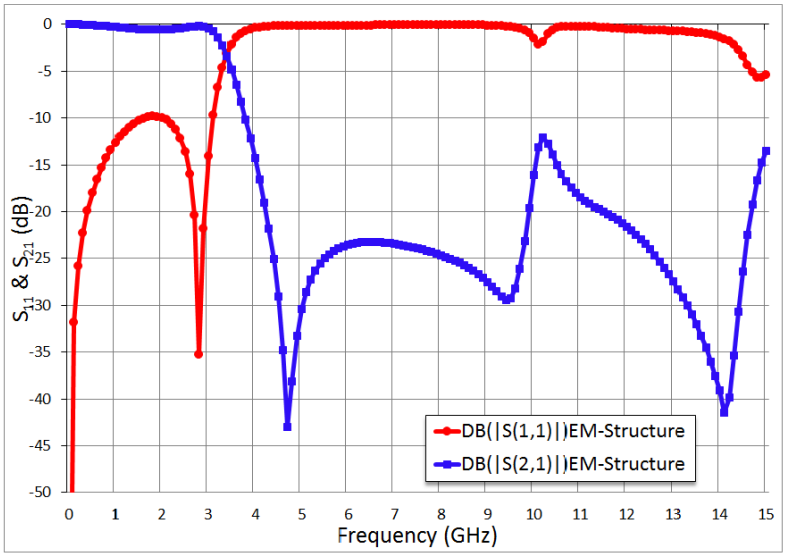

Figure 10. Simulation results of the proposed LPF structure.

at 3.45 GHz and 3.30 GHz and first attenuation poles at 6.57 GHz and 4.75 GHz, respectively.

As shown in Fig. 11, the sharpness factor of the transformed filter is 34 dB/GHz at transition knee, rejection better than 20 dB from 3.5 GHz up to 11.5 GHz, and the insertion loss in the passband about 0.3 dB. Thus, it is demonstrated that the proposed Π-H-Π shaped DGS lowpass filter with its new topology has a good performance.

4. EM FIELD DISTRIBUTION IN THE PASS- AND STOP-BANDS

The investigation of this EM field distribution has the objective of showing the frequency behaviour of this proposed filter and to prove the validity of the intuitive equivalent circuit. Fig. 12(a) shows the field distribution in the passband region at the frequency of 1.5 GHz. Around this frequency almost the whole RF magnetic energy was transmitted from the input to the output using the compensated patch capacitors, which are electrically coupled with both the DGS slots in the ground plane. The

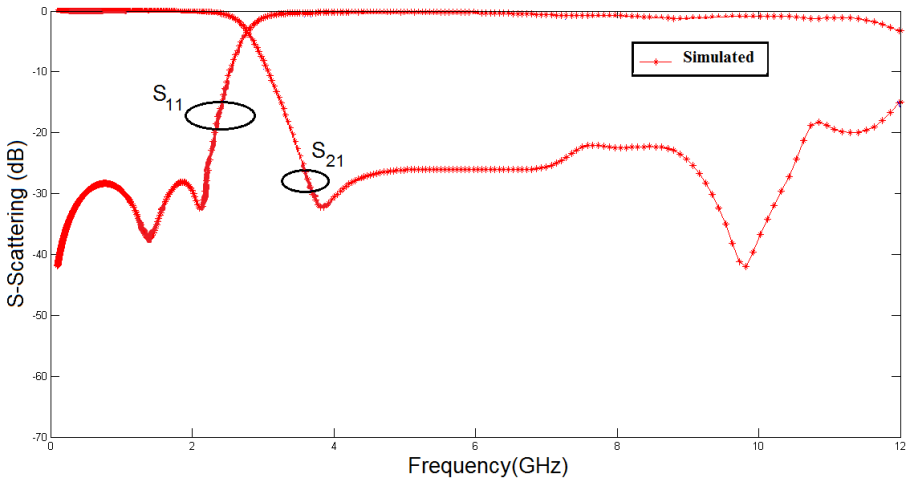

Figure 11. The scattering parameters of simulated LPF structure.

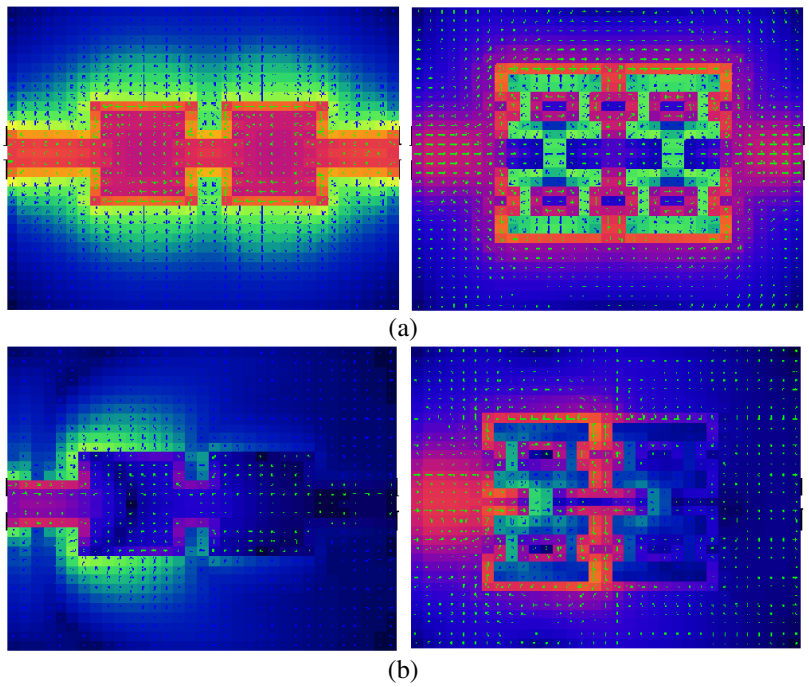

Figure 12. Electromagnetic field distribution results: (a) in the pass-band at 1.5 GHz and (b) in the stop-band at 4.5 GHz.

magnetic field is concentrated along the DGS-resonators and on the 50 Ω lines, while a negligible electric field appears between channels of the DGS shapes. The transmission power between the two ports is magnetic. The windows of the DGS represent inductance. Fig. 12(b) shows a filter with stopband behaviour at a resonant frequency of 4 GHz. At this frequency, the flux-energy is blocked at the input of the structure. The electric and magnetic fields show equal distribution densities. The electric field is concentrated between the channels of the first DGS resonator, which represents the capacity. This behaviour indicates that the structure is in the stopband state, and more precisely, the structure undergoes a resonance effect as shown in Fig. 12(a). Based on this EM field investigation, the parallel LC circuit can be a approach model for the DMS unit.

5. FABRICATION AND MEASUREMENTS OF THE Π-H-Π LOWPASS FILTER

In order to increase the sharpness factor of the structure and thus to improve the stopband, two shaped DGSs were introduced. Dimensions of the identical DGS resonators are marked in Figs. 1 and 9. The adding of the rectangular microstrip metal in the DGS-window leads to a suppression of the scattering S_{11} in the low frequency range. The compensated patch capacitors caused a significantly improvement of the insertion loss in the passband, especially near the cutoff frequency, see Fig. 11. The proposed LPF was fabricated using substrate Rogers RO4003 with dielectric constant of 3.38, thickness of 0.813 mm and dielectric loss tangent (δ) = 0.0027 shown in Figs. 13(a) and (b). The feeding microstrip line width is equal to 2 mm to have a characteristic impedance of 50 Ω. The fabricated filter is tested and measured using HP8722D network analyzer, and the results are depicted in Fig. 14. As a reference, the measured and simulated results are shown as blue dot and red square lines. It can be seen that the measured results agree well with the simulated ones. The 3 dB cutoff frequency of the filter is equal to 3 GHz. Insertion loss is less than 0.83 dB in the passband, while the suppression level is higher than 20 dB from 3.5 GHz to 11.5 GHz. The measurement results exhibit sharp roll-off (ξ) of 34 dB/GHz, and the structure occupies an area of ($0.370\lambda g \times 0.370\lambda g$) with $\lambda g = 54.4$ mm. The features of the proposed Π-H-Π lowpass filter as well as that of other reported LPFs are depicted in Table 2. This work shows that the proposed filter provides good performance in stopband rejection and passband insertion loss

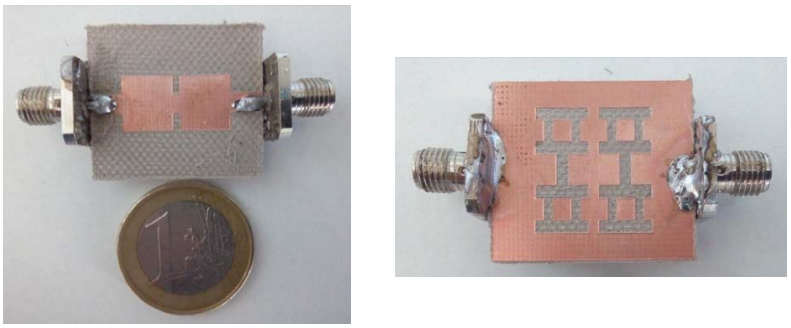

(a) (b)

Figure 13. Photograph of the fabricated open-loop-ring DGS BSF: (a) top view, (b) bottom view.

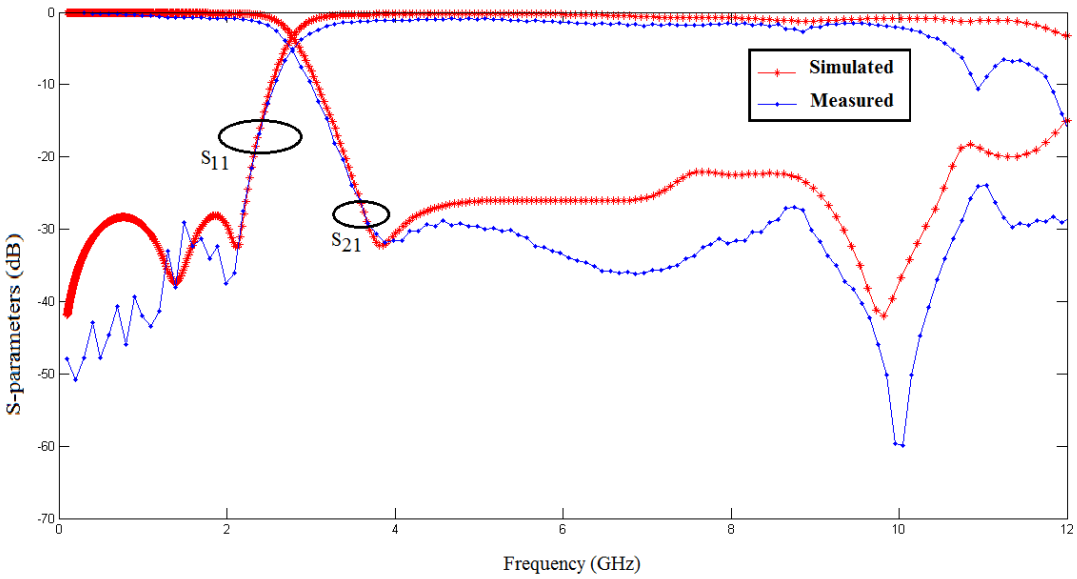

Figure 14. Measured and simulated S-parameters of the proposed LPF.

Table 2. Comparison of performance of proposed low-pass filter with various related LPF.

Ref.	(ξ) (dB/ GHz)	Size (mm^2)	f_c (GHz)	Stopband (GHz) with -20 dB	Inserion Loss ($S_{21} < -20$ dB)	RL ($S_{11} < -20$ dB)
[17]	14.16	15×10	3.40	4.5–17	0.3	> 23
[18]	11.33	27×21	2.95	5.0–15	0.4	> 20
[19]	34.00	71×13	2.40	2.8–10	2.0	> 10
[20]	42.50	45×45	2.50	2.7–4.6	1.0	> 12
This work	**34.00**	$\mathbf{20 \times 20}$	**3.00**	**3.5–11.5**	**0.3**	$\mathbf{> 28}$

and is smaller in size ($20 \times 20\,mm^2$) than those reported in literature.

$$\lambda_g = \frac{\lambda}{\sqrt{\varepsilon_{r,eff}}} = 0.54\left(\frac{c}{f_0}\right) \tag{14}$$

$$\xi(selectivity) = \frac{\alpha_{\min} - \alpha_{\max}}{f_0 - f_c}\ (\text{dB/GHz}) \tag{15}$$

where ξ = filter selectivity in dB/GHz, $\alpha_{\max}$ = the 3 dB attenuation point, $\alpha_{\min}$ = attenuation at f_0, $f_s = f_0$ (attenuation pole) and $f_c = 3$ dB cutoff frequency.

6. CONCLUSION

In this paper, the design and implementation of a compact Π-H-Π lowpass filter with wide reject band features using defected ground structure DGS technique has been presented. Two compensated capacitors are placed on the top layer to minimise the loss in passband. The two DGS resonators are each electromagnetically coupled to each other, and electrically coupled with the elements placed on the top layer. Employing this technique, very compact filter topology with design flexibility and excellent results are achieved. The size of the proposed Π-H-Π lowpass filter is less than ($0.370\lambda_g \times 0.370\lambda_g$) with $\lambda_g = 54.4$ mm. Experimental measurements by means of HP8719D network analyser agree well with simulated results which are obtained by Microwave Office. The slight discrepancy between two results can be attributed to unexpected tolerance errors in fabrication and manual welding inaccuracies. Such topologies can be easily integrated with RF-, as well as wireless mobile systems which require compact and wide reject band filters.

ACKNOWLEDGMENT

The first author thanks the German Research Foundation (DFG) for financial support. The author thank M. Sc. Eng. Sonja Boutejdar, Mehdi Boutejdar, Karim Boutjdir, Mohamed Boutejdar for their assistance and University of Boumerdes, Institute of Electrical Engineers and Electronics (IGEE, Ex. INELEC), Dept. of Electronics, Boumerdes, Algeria for its help in fabrication.

REFERENCES

1. Wang, C. J. and C. H. Lin, "Compact lowpass filter with sharp transition knee by utilizing a quasi-π-slot resonator and open stubs," *IET Microwaves Antennas & Propagation*, Vol. 4, 512–517, 2010.
2. Cui, H., J. Wang, and G. Zhang, "Design of microstrip low pass filter with compact size and ultra-wide stopband," *Electronics Lett.*, Vol. 48, 856–857, 2012.
3. Ma, K. and K. S. Yeo, "New ultra-wide stopband low-pass filter using transformed radial stubs," *IEEE Trans. Microw. Theory Techn.*, Vol. 59, 604–611, 2011.

4. Raphika, P. M., P. Abdulla, and P. M. Jasmine, "Compact lowpass filter with a sharp roll-off using patch resonators," *Microw. and Opt. Tech. Lett.*, Vol. 56, 2534–2536, 2014.
5. Raphika, P. M., P. Abdulla, and P. M. Jasmine, "Compact microstrip lowpass filter with sharp roll-off and wide stopband by cascading multiple resonators," *Proceedings of Asia Pacific Microwave Conference*, 1229–1231, Japan, 2014.
6. Ge, L., J. P. Wang, and Y.-X. Guo, "Compact microstrip lowpass filter with ultra-wide stopband," *Electronics Lett.*, Vol. 46, No. 10, 689–691, 2010.
7. Li, L., Z.-F. Li, and J.-F. Mao, "Compact lowpass filters with sharp and expanded stopband using stepped impedance hairpin units," *IEEE Microwave Wireless Compon. Lett.*, Vol. 20, No. 6, 310–312, 2010.
8. Xiao, M., G. Sun, and X. Li, "A Lowpass filter with compact size and sharp roll-off," *IEEE Microwave Wireless Compon. Lett.*, Vol. 25, No. 12, 790–792, 2015.
9. Boutejdar, A., "Design of a very compact U-HI-LO low-pass filter using meander technique and quasi horn inductors for L-band and C-band applications," *Microw. and Opt. Tech. Lett.*, Vol. 58, No. 12, 2897–290, 2016.
10. Boutejdar, A., A. Omar, and E. Burte, "High-performance wide stop band lowpass filter using a vertically coupled DGS-DMS-resonators and interdigital capacitor," *Microw. and Opt. Tech. Lett.*, Vol. 56, 87–91, 2014.
11. Boutejdar, A., et al., "Design of a novel ultrawide stopband lowpass filter using a DMS-DGS technique for radar applications," *International Journal of Microwave Science and Technology*, Vol. 6, 1–7, 2015.
12. Boutejdar, A., "A new approach to design compact tunable BPF starting from simple LPF topology using a single T-DGS-resonator and ceramic capacitors," *Microw. and Opt. Tech. Lett.*, Vol. 58, No. 5, 1142–1148, 2016.
13. Yang, M. H., J. Xu, Q. Zhao, L. Peng, and G. P. Li, "Compact, broad stopband lowpass filters using SIRs-loaded circular hairpin resonators," *Progress In Electromagnetics Research*, Vol. 102, 95–106, 2010.
14. Chan, H. and K. C. Kai, "Independently controllable dual band BPF using asymmetric stepped impedance resonator," *IEEE Trans. Microw. Theory Techn.*, Vol. 59, 3037–3047, 2011.
15. Chen, W.-Y., M.-H. Weng, S.-J. Chang, H. Kuan, and Y.-H. Su, "A new tri-band bandpass filter for GSM, WiMAX and ultra-wideband responses by using asymmetric stepped impedance resonator," *Progress In Electromagnetics Research*, Vol. 124, 365–381, 2012.
16. Challal, M., A. Boutejdar, M. Dehmas, A. Azrar, and A. Omar, "Compact microstrip low-pass filter design with ultra-wide reject band using a novel quarter-circle DGS shape," *Appl. Comp. Electro. Society (ACES) Journal*, Vol. 27, No. 10, 808–815, Oct. 2012.
17. Al-Omair, G. E., S. F. Mahmoud, and A. S. AlZayed, "Lowpass and bandpass filter designs based on DGS with complementary split ring resonators," *Appl. Comp. Electro. Society (ACES) Journal*, Vol. 26, No. 11, 907–914, Nov. 2011.
18. Boutejdar, A., "New method to transform bandpass to lowpass filter using multilayer- and U-slotted ground structure-technique," *Microw. and Opt. Tech. Lett.*, Vol. 53, 2427–2433, 2011.
19. Boutejdar, A., A. Omar, and E. Burte, "LPF builds on quasi-yagi DGS," *Microwaves & RF*, Vol. 52, 72–77, 2013.
20. Boutejdar, A., "Design of broad stop band low pass filter using a novel quasi-Yagi-DGS resonators and metal box technique," *Microw. and Opt. Tech. Lett.*, Vol. 56, No. 3, 523–528, 2014.
21. Mandal, M. K. and S. Sanyal, "A novel defected ground structure for planar circuits," *IEEE Microwave Wireless Compon. Lett.*, Vol. 16, No. 2, 93–95, 2006.
22. Boutejdar, A., "Design of compact reconfigurable broadband band-stop filter based on a low-pass filter using half circle DGS resonator and multi-layer technique," *Progress In Electromagnetics Research C*, Vol. 71, 91–100, 2017.